Science Bulletin 65 (2020) 225–232

Contents lists available at ScienceDirect

Science Bulletin

journal homepage: www.elsevier.com/locate/scib

Article

A leaf vein-like hierarchical silver grids transparent electrode towards high-performance flexible electrochromic smart windows

Teng Li [a,b,1], Shengyou Li [a,b,1], Xuyi Li [a,b], Zijie Xu [a,b], Jizhong Zhao [a,b], Yating Shi [a,b], Yanan Wang [a,b], Rui Yu [a,b], Xiangyang Liu [a,c], Qingchi Xu [a,b,*], Wenxi Guo [a,b,*]

[a] Shenzhen Research Institute of Xiamen University, Shenzhen 518057, China
[b] Research Institute for Soft Matter and Biomimetics, Department of Physics, Jiujiang Research Institute, Xiamen University, Xiamen 361005, China
[c] Department of Physics, Faculty of Science, National University of Singapore, Singapore 117542, Singapore

ARTICLE INFO

Article history:
Received 4 September 2019
Received in revised form 27 October 2019
Accepted 20 November 2019
Available online 30 November 2019

Keywords:
Flexible transparent conductive electrodes
Hierarchical grids
Crackle pattern
Electrochromic device

ABSTRACT

As essential components of numerous flexible and wearable optoelectronic devices, the flexible transparent conducting electrodes (TCEs) with sufficient optical transmittance and electric conductivity become more and more important. In this work, we fabricated a large-area flexible TCE based on leaf vein-like hierarchical metal grids (HMG) comprising of mesoscale "trunk" and microscale "branches". The self-formed branched grids made the conducting paths distributing uniformly while the laser-etching trunk grids enabled to transport the collected electrons across long-distance. The Ag HMG exhibited high optical transmittance (~81%) with low sheet resistance (1.36 Ω sq^{-1}), which could be simply optimized through adjusting the grids' widths, spaces, and the sizes of the TiO_2 colloidal crackle patterns. In addition, on the basis of such advanced HMG electrode, flexible electrochromic devices (ECDs) with remarkable cyclic performance were fabricated. The HMG with high transparency, conductivity, and flexibility provides a promising TCE for the next-generation flexible and wearable optoelectronic devices.

1. Introduction

Over the past years, flexible transparent conductive electrodes (TCEs) have attracted great attention due to their wide applications in flexible optoelectronic devices, such as flexible touch panels, flexible displays, wearable sensors, and electrochromic smart windows [1–5]. Conventionally, transparent conductive oxides, such as fluorine-doped tin oxide (FTO) and indium tin oxide (ITO), are the most widely used materials for transparent conductors (TCO), which have desirable optoelectronic performance [6,7]. However, there are many disadvantages, containing low infrared transmittance, film brittleness, low abundance, and the high cost of high-quality ITO, restricting its applications in the next-generation flexible and wearable electronics [8–10].

In recent years, possible alternatives such as conducting polymers [11], carbon materials [12–14], and metal networks [15,16] have been employed as conductive materials for charge transport after being assembled on flexible and transparent substrates. Among these candidates, the metal grids exhibit excellent electrical and optical properties which are even superior to ITO [17,18]. Flexible TCEs based on metal grids have also been a desirable option because both their resistance and transmittance can be easily controlled by adjusting the grids widths, spaces, and thickness [19–23]. However, large-area insulating open spaces among the metal grids would increase the contact resistance between the network and active materials, limiting their applications in display, electrochromism or touch screen [24,25]. Some composite electrodes, such as reduced graphene oxide/metal grids and poly 3,4-ethoxythiophene (PEDOT:PSS)/metal grids, have been employed to increase the conductivity [26,27]. Based on graphene-metal nanowire hybrid structures, Lee et al. [28] fabricated a flexible composite TCE with high optoelectronic performance (33 Ω sq^{-1}, 94% T (transmittance)) and superior mechanical flexibility. However, the chemical vapor deposition process involved in this work limited its applications. In this context, to reduce the open spaces among the metal grids, constructing multiple-scale metal networks on flexible substrates is another way to fabricate high-performance ITO-free TCEs [29]. Cui and co-workers [30] proposed a mesoscale metal-wire concept in conjunction with metal nanowire TCEs to demonstrate at least a one order of magnitude reduction in sheet resistance at a given transmittance. As for the fabrication method, the annealing step is necessary and the three different steps for fabricating this hybrid material make the whole process complexity. Therefore, it is neces-

* Corresponding authors.
E-mail addresses: xuqingchi@xmu.edu.cn (Q. Xu), wxguo@xmu.edu.cn (W. Guo).
[1] These authors contributed equally to this work.

https://doi.org/10.1016/j.scib.2019.11.028
2095-9273/

sary to search some rational methods to fabricate the flexible TCEs with good optoelectronic performance by simple, cheap, and large-scale methods. Inspired by the leaf-veins with numerous typical micro-nano scaffolds, Gao and co-workers [31,32] proposed a flexible TCE with quasi-fractal structure derived directly from a chemically extracted leaf venation system, demonstrating an exceptional optoelectronic and mechanical performance. However, the irregular nature of the venation network leads to large uncertainty in the performance.

In this work, a simple and low-cost method was employed to large-area fabrication of leaf vein-like HMG comprising of mesoscale "trunk" and microscale "branches". The microscale "branches" were prepared by self-formed crackle template method. The colloidal solution dropped on a substrate was utilized as sacrificial layer and allowed to dry so that it would spontaneously crack and form a single network of highly interconnected cracks over the substrate [33]. The self-formed technique is simple and suitable for mass production of TCEs. However, compared with traditional lithography techniques, some defects (such as breaks and uncompleted cracks) are inevitable, especially in large-scale film. In this context, the mesoscale metal-grids are further constructed on the aforementioned self-formed TCEs by simply laser etching the cracked pattern. The flexible TCE based on HMG comprising of mesoscale lines (40–100 μm) and fine cracks (3–10 μm) demonstrated a sheet resistance of 1.36 Ω sq^{-1} with 81% *T*. In addition, on the basis of such advanced HMG electrode, high stable flexible electrochromic devices (ECD) were fabricated as smart windows.

2. Experimental

2.1. Materials

TiO_2 was provided by Degussa Co. (Germany). Propylene carbonate (PC, 99.7%), ethanol (99.8%), ethyl acetate (99.5%) and $LiClO_4$ (99.9%) were supplied from Aladdin Co. (China). The 0.02-mm thick polyethylene terephthalate (PET) films are commercially purchased. All chemicals used were not further purified. Ag target (99.99%) and WO_3 target (99.99%) were provided by Zhongnuoxincai (Beijing) Technology Co. (China).

2.2. Preparation of the hierarchy TCF

Fig. 1 illustrates the key steps of the WO_3/Ag HMG electrodes producing process. Firstly, commercial TiO_2 particles (P25, Degussa AG) were chosen as the colloidal pattern materials. They were dispersed into ethyl alcohol (2 mol L^{-1}) and some ethyl acetate by ultrasonic vibration (40 min). Secondly, the mixed colloidal solution was dropped uniformly on a pre-cleaned flat PET substrate (10–30 mL cm^{-2}) (Fig. 1a). Then, the uniform crackle patterns were obtained after drying in ambient condition (Fig. 1b). After the microscale cracks formed on all over the substrate, laser beam was utilized to equidistantly cut mesoscale lines (40–100 μm) that is much wider than fine cracks (3–10 μm), as shown in Fig. 1c. Then, magnetron sputtering was applied to deposit WO_3 and Ag into the cracks in the pattern to form a WO_3/Ag conductive network (60 W, 0.5 Pa in argon-shield atmosphere, direct-current power supply). Tungsten trioxide (WO_3, 30 nm thick) was deposited as bottom layer before Ag was deposited on the crack template as conducting layer (Fig. 1d, e). Finally, the TiO_2 colloidal pattern was removed by weak ultrasonic vibration to obtain the HMG electrodes (Fig. 1f).

2.3. Characterizations

All physical photos were taken by digital single lens reflex (DSLR) Camera. The morphological and microscale properties of the TCFs were measured through a field-emission scanning electron microscope (SEM, Hitachi SU-70, Japan). The transmittance of the TCFs was measured by UV–vis-NIR spectroscope (Lambda 750, Perkin Elmer, USA) with a spectral wavelength in a range of 400–800 nm, and the PET was used as a reference material. A four-point probe instrument (RST-8) was used to measure the sheet resistance (R_s). X-ray diffraction (XRD) was carried out on a Bruker D8 powder diffractometer using a Cu Kα source (λ = 1.5418 Å) at 40 kV and 30 mA. X-ray photoelectron spectroscopy (XPS) was performed on an Escalab 250Xi XPS microscope. A computer-controlled CHI 660e electrochemical work station (Shanghai Chenhua Instruments Inc., China) was applied in all the electrochemical measurements with a three-electrode system which consists of the 1 mol L^{-1} $LiClO_4$/PC solution as electrolyte, the Hg/Hg_2Cl_2 (1 mol L^{-1} KCl) electrode as the reference and a platinum plate as the counter electrode in a room temperature.

3. Results and discussion

The image of the obtained flexible WO_3/Ag HMG film on PET with a size of (13 × 9) cm^2 is displayed in Fig. 2a, demonstrating high transmittance from the naked eyes. The magnified optical microscopy and SEM images of this WO_3/Ag HMG film before and after removing the TiO_2 colloid templates are shown in Fig. 2b, c, respectively, demonstrating that the TiO_2 colloidal is uniformly self-cracked all over the film and all the TiO_2 colloidal templates are removed after magnetron sputtering of WO_3 and Ag. The crackle grid width (3–10 μm) can be controlled by the colloid concentration, drying temperature, colloid dosage, drying rate and ambient humidity. After the laser etching, micron-sized grids ranging from 40 to 100 μm can be obtained on the resulting crackle patterns. Fig. S1 (online) shows the line width variation according to different laser scanning speeds and laser powers. The micron-sized grids can be easily designed into arbitrary shapes (e.g., hexagon, square, triangle) by drawing software. Fig. 2d displays the WO_3 compact layer was uniformly pre-sputtered on the PET substrate to enhance the adhesion [34]. Hierarchical networks are readily found in many biological systems, i.e., insect wing or leaf venations, they have various kinds of functions which include being a support for mechanical cellular integrity, nutrients distribution via microfluidic channels. Fig. 2f presents a typical hierarchical network in the Pachira macrocarpa leaf with multi-scale veins. The "trunks" in the leaf emanate numerous smaller branches to form uniform network on all over the leaf, which is benefit for nutrients transport. Compared with the natural hierarchical networks, our HMG film as shown in Fig. 2e demonstrates similar configuration comprising of mesoscale "trunk" and microscale "branches".

The influence of the grid shapes on the optical transmittance of the HMG was investigated by designing regular triangles, squares and regular hexagons shaped grids as shown in Fig. 3a–c. To simplify the discussion, it is assumed that the metal grids are opaque, and the blank portion of the substrate is completely transparent. If the line widths of the three types of graphics are represented by 2*a* and the length of the side is denoted by *g*, then the theoretical light transmission can be calculated as follows [35]:

$$T_{\text{triangle}}\% = \frac{\frac{\sqrt{3}}{4}g^2 - 6ag}{\frac{\sqrt{3}}{4}g^2 - 3ag} \times 100\%, \quad (1)$$

$$T_{\text{square}}\% = \frac{(g-4a)^2}{(g-2a)^2} \times 100\%, \quad (2)$$

$$T_{\text{hexagon}}\% = \frac{\frac{3\sqrt{3}}{2}g^2 - 12ag}{\frac{3\sqrt{3}}{2}g^2 - 6ag} \times 100\%. \quad (3)$$

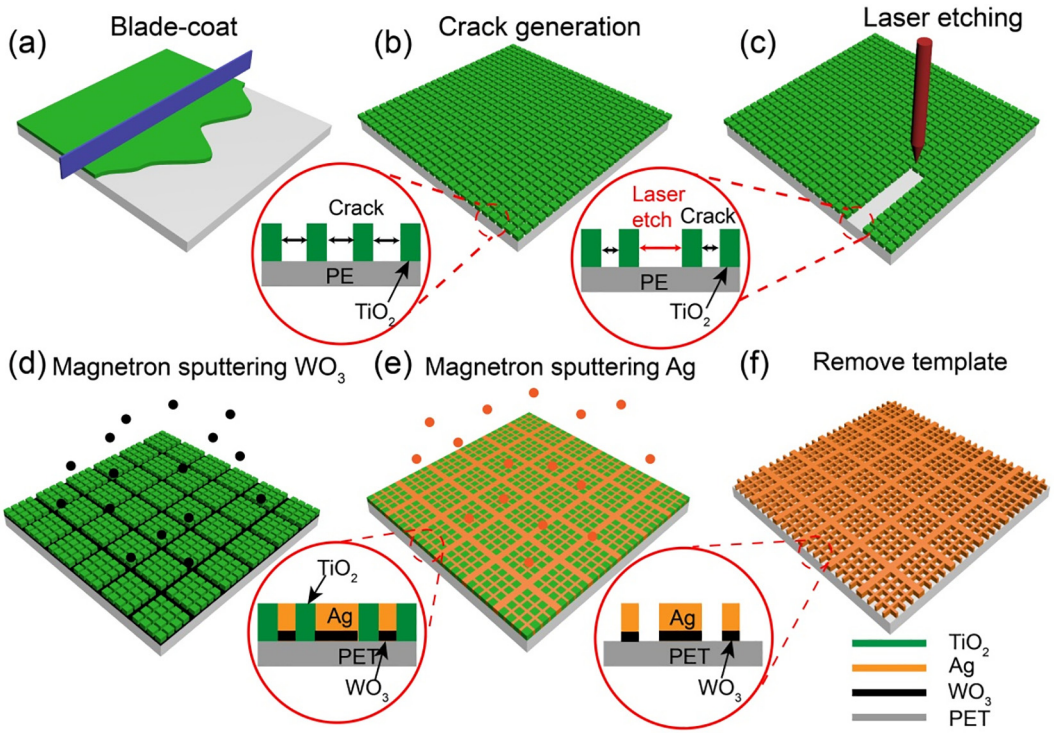

Fig. 1. (Color online) Schematic of the procedures of manufacturing the WO_3/Ag hierarchical metal grids electrode. (a) TiO_2 colloidal solution was coated on a PET substrate uniformly by using a blade. (b) Microscale crackles were formed naturally by solvent evaporating in the air. (c) Using the laser beam to form the mesoscale patterns. Depositing WO_3 (d) and Ag (e) on the crackle template sequentially through magnetron sputtering method. (f) Removing TiO_2 patterns through soft ultrasonic vibration.

According to the aforementioned formulas, the theoretical optical transmittance as a function of side length is shown in Fig. 3d when the line width is 50 μm. As expected, for all samples, the transmittance increased with the increasing gird width. The order of optical transmittance for the three TCFs at any side length (300–1000 μm) goes hexagonal grids > square grids > equilateral triangle grids. As we know, the larger area-to-length ratio allows the higher light transmittance with the minimum total length of the line. According to Eqs. (1)–(3), obtaining the same theoretical optical transmittance, the TCFs with hexagon grids required smaller side length than the other two TCFs. When the grid line width is 50 μm and the transmittance is 90%, the required length for the regular triangle is 1900 μm, the square is 1050 μm and the hexagon is 635 μm, respectively, indicating that the regular hexagonal grid has a shape advantage that ensures maximum light transmittance. Further investigation was performed to recognize the effect of variations in grid line width on optical transmittance. As exhibited in Fig. 3e, it is clear that the optical transmittance of all the samples decreases continuously as the grid line width increases. Relatively speaking, the decreasing rate of optical transmittance for TCFs based on the hexagonal grids is the lowest. The aforementioned three hierarchical TCFs with similar transmittance (~80%) were fabricated as shown in Fig. 3f. As expected, the regular hexagonal shows the smallest sheet resistance while the regular triangle shows the largest one, which totally agrees with the theoretical calculation.

$$\mathrm{FoM} = \frac{\sigma_{dc}}{\sigma_{opt}} = \frac{188.5}{R_s\left(\frac{1}{\sqrt{T}} - 1\right)}. \quad (4)$$

The figure-of-merit (FoM) is defined as Eq. (4) [36] to value the overall performance of the TCF, where σ_{dc} is the electrical conductivity and σ_{opt} is the optical conductivity. The quality factors of the three grid films are 1247.4 (hexagon, T = 81%, R_s = 1.36 Ω sq^{-1}), 643.1 (square, T = 80.7%, R_s = 2.59 Ω sq^{-1}) and 377.2 (triangle, T = 80.3%, R_s = 4.31 Ω sq^{-1}), respectively. The results further prove that the hexagonal HMG film has the best light transmission and electrical conductivity properties under the same grid line width and theoretical light transmittance.

In the application, compared with traditional lithography techniques, some defects (such as breaks, uncompleted cracks) inevitably exist in self-formed crackle template TCF, especially in large-scale film (Fig. 4b, c). In this context, trunk conducting paths are urgent needed to collect the electrons from cracked branches to remote electrons transport, as shown in Fig. 4d. The self-formed branched grids made the conducting paths distributing uniformly while the laser-cutting trunk grids collected the electrons for long-distance transport. To further demonstrating the importance of the HMG concept, long strip shaped crackle template TCF (10 cm × 1 cm) with and without hexagonal mesoscale grids were prepared, as shown in Fig. 4a. The relationship between the resistance and the length of conductive film by increasing the distance of 1 cm at one time is shown in Fig. 4e. Obviously, the resistance of the crackle conductive film increases nonlinearly due to the existing of the defects, while the resistance of the hierarchical grids conductive film increases approximately linearly with the increase of the length, demonstrating that the mesoscale metal grid enhances the stability and uniformity of the crackle pattern conductive film.

The mechanical properties of the as-prepared WO_3/Ag HMG film were investigated. Fig. 5a illustrates the variations in R_s of Ag hierarchical grids (HG), WO_3/Ag HG and ITO/PET film as the function of the number of bending cycles at a bending radius of 1 mm. It is obvious that only 4.56% increase in R_s of WO_3/Ag HMG film while about 802% increase in that of the commercialized ITO/PET films after 500 bending cycles, indicating the good cycling performance of WO_3/Ag HMG film. Furthermore, it is obvious that WO_3/Ag HMG conductive film has good mechanical flexibility, and

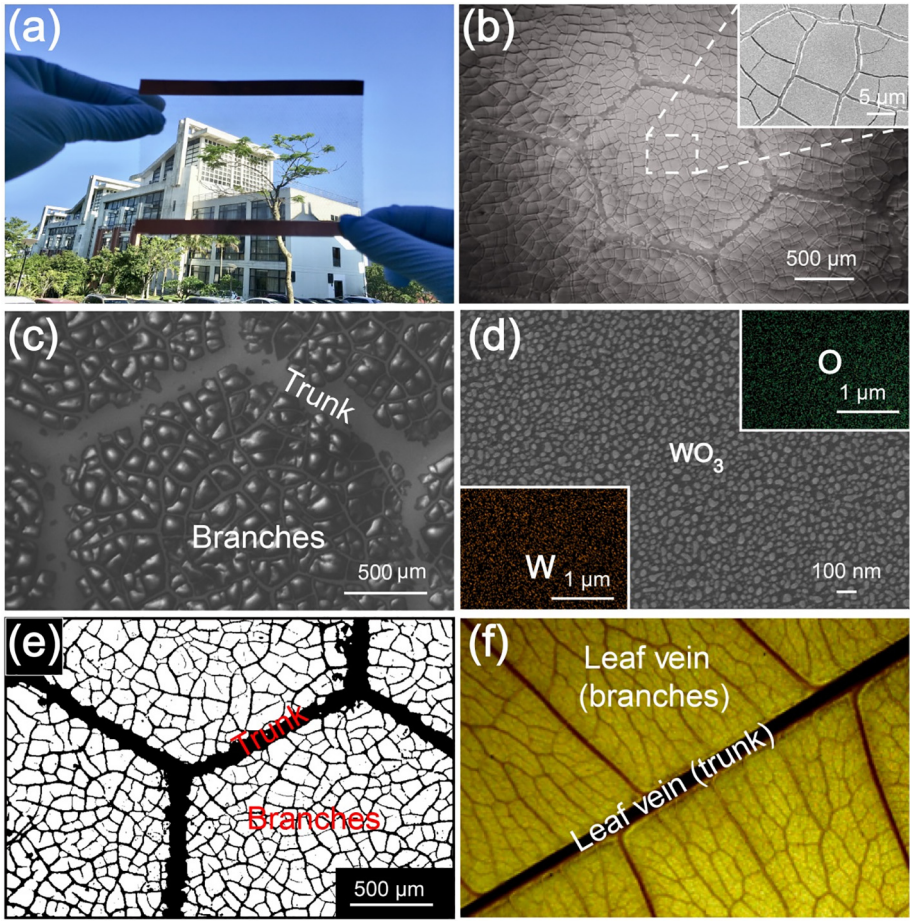

Fig. 2. (Color online) (a) The photograph of a typical flexible WO_3/Ag HMG film (R_s is 1.36 Ω sq^{-1}, T = 81%). (b) SEM images of the TiO_2 colloid pattern and the inset displays the magnified crack pattern. (c) SEM image of the flexible WO_3/Ag HMG film after getting rid of the TiO_2 templates. (d) SEM image of the WO_3 electrochromic layer and the corresponding EDS mapping for elements O and W. (e) Optical microscopy image of the flexible WO_3/Ag HMG film after removing the colloid templates. (f) The photograph of a typical hierarchical leaf structure.

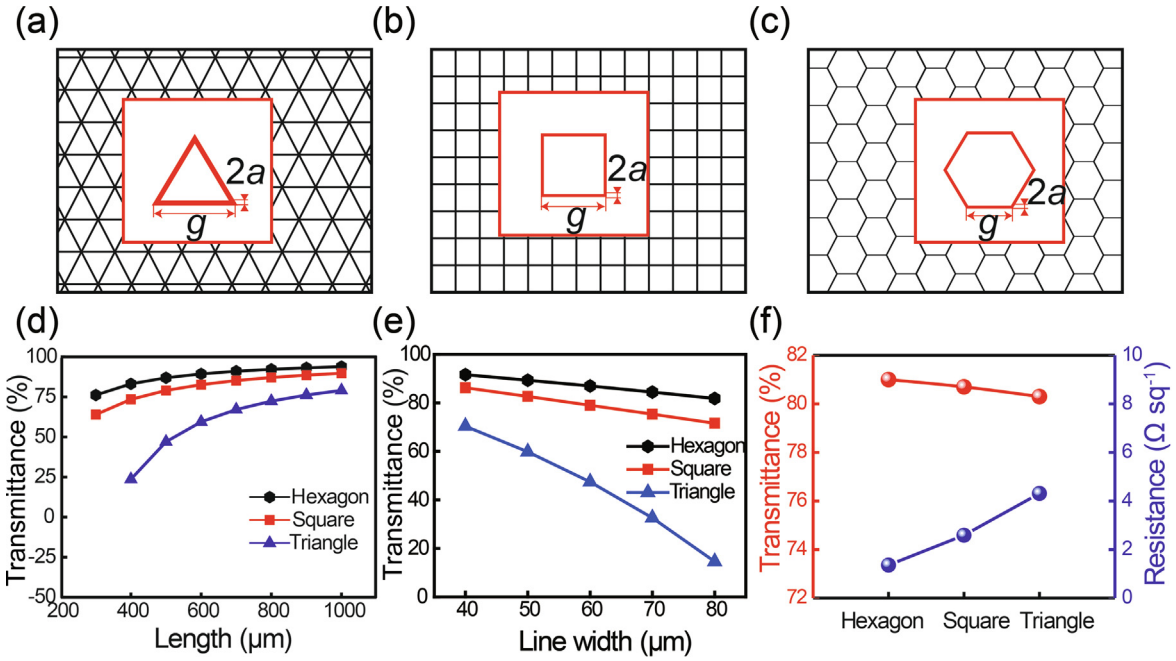

Fig. 3. (Color online) Schematic of the triangle (a), square (b), and hexagon (c) structural metal grids, respectively. (d) Optical transparency of metal grids with different side lengths when the line width is 50 μm. (e) Optical transparency of metal grid with different line widths when the side length is 600 μm. (f) Optical transparency and sheet resistances of the three kinds of WO_3/Ag HMG electrode.

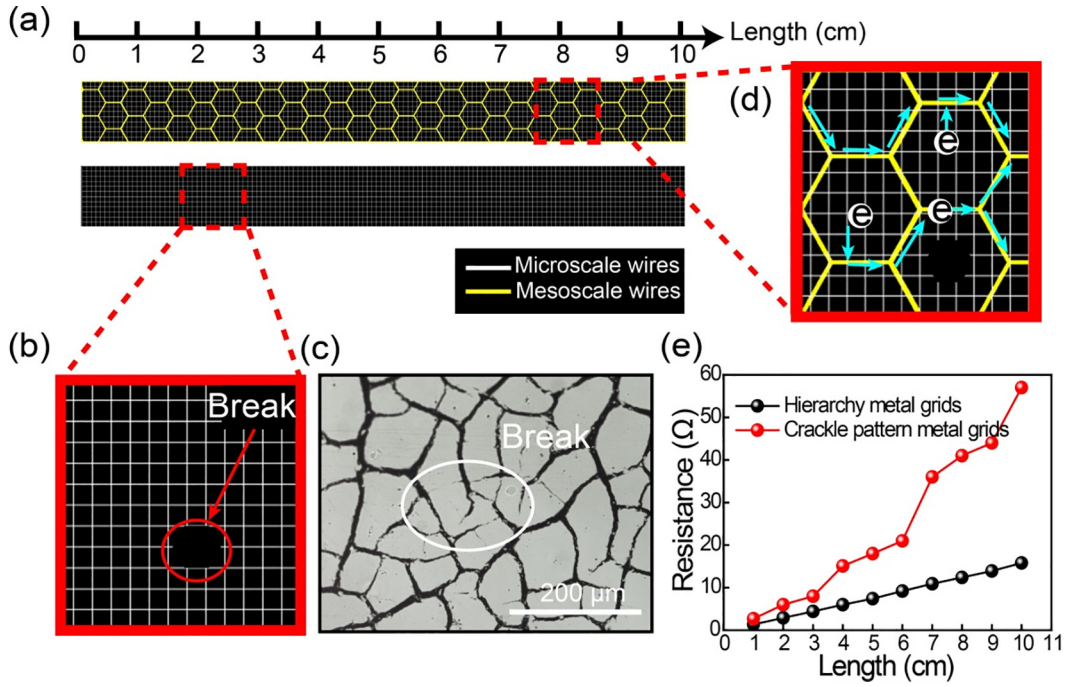

Fig. 4. (Color online) The comparison of the crackle template conductive film and hierarchical grids conductive film. (a) Crackle template conductive film and hierarchical grids conductive film with the size of 10 cm × 1 cm. (b) High-magnification view of the crackle template conductive film. (c) Optical microscopy image of the crackle template conductive film. (d) High-magnification view of hierarchical grids film. (e) The relationship between resistance and measuring length of the TCFs.

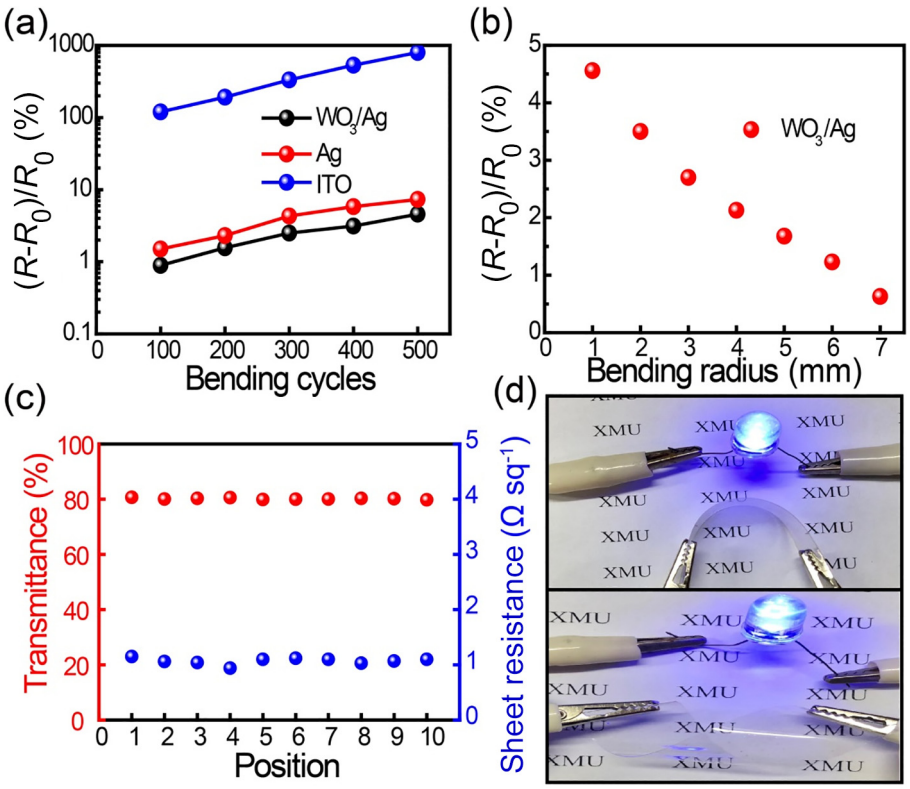

Fig. 5. (Color online) The relative variations in resistance of as-prepared TCEs during (a) 500 bending cycles to radius of 1 mm, and (b) bending to different radii. (c) Sheet resistance and transmittance measured across 400 cm^2 area of WO_3/Ag FTCEs prepared from one template. Each measurement was done over 30 mm × 20 mm randomly chosen areas. (d) Digital photographs of working LED connect with bending and twisting TCEs which acted as a segment of external circuits after 500 times twisting tests.

the variations in resistance are very small during the deformation. The variations in R_s of WO_3/Ag HMG film as a function of different bending radii were recorded as shown in Fig. 5b. When the bending curvature was greater than 7 mm, the variations in R_s after bending 500 times was less than 0.6%. When the bending curvature was less than 1 mm, the variation in R_s of the WO_3/Ag HMG film after bend-

ing for 500 times was only 4.56%. To investigate the uniformity of the WO_3/Ag HMG film, we divided a 20 cm × 20 cm WO_3/Ag HMG film into 10 pieces with the same size (2 cm × 3 cm) for transmittance and sheet resistance measurement, respectively. As can be seen from Fig. 5c, the transmittances of all the samples were almost the same in the sheet resistances and transparency, indicating superior uniformity of the HMG conducting film. Fig. 5d shows the photographic images of working LED with bending WO_3/Ag HG electrodes as segments of external circuits, demonstrating that our conductive film remains conductive during bending.

The flexible EC electrode with sandwich structure of WO_3/Ag/WO_3 was prepared by magnetron sputtering of WO_3 on the WO_3/Ag HMGs electrode, as shown in Fig. 6a. XRD and XPS characterizations have been introduced to further investigate the component and structure of the electrochromic and conducting layers. As shown in Fig. S2a, b (online), the diffraction peaks located at 23.6°, 33.6°, and 38.3° are index to (2 0 0), (2 2 0), and (1 1 1) of WO_3 and Ag, respectively. XPS spectra of the WO_3 and Ag are shown in Fig. S2c, d (online), respectively. Two peaks located at 35.6 and 37.7 eV in Fig. S2c (online) are index to W 4f of WO_3, which could be assigned as W(VI) $4f_{7/2}$, W(VI) $4f_{5/2}$ respectively. The Ag $3d_{5/2}$ peaks for our samples are positioned at 367.5 eV in Fig. S2d (online) that corresponds to Ag states. Fig. 6b shows the photos of the flexible EC electrode in bleached and colored status. Fig. 6c illustrates the cyclic voltammetry (CV) curves of the flexible EC electrode at the scan rates of 10–110 mV s^{-1} under a potential window ranging from –1.4 to 0.2 V. According to the CV curves, the WO_3 redox peaks could be maintained even at a high scan rate, which means a rapid redox reaction of WO_3 and a pseudocapacitance of the supercapacitor. Fig. 6d recorded 1st, 1000th, 2000th and 3000th cycles in 1 mol L^{-1} $LiClO_4$ + PC solution with a scanning rate of 10 mV s^{-1} between –1.4 and 0.2 V at room temperature. The corresponding reaction process can be described as follows

$$WO_3 + xLi^+ + xe^- \leftrightharpoons Li_xWO_3$$

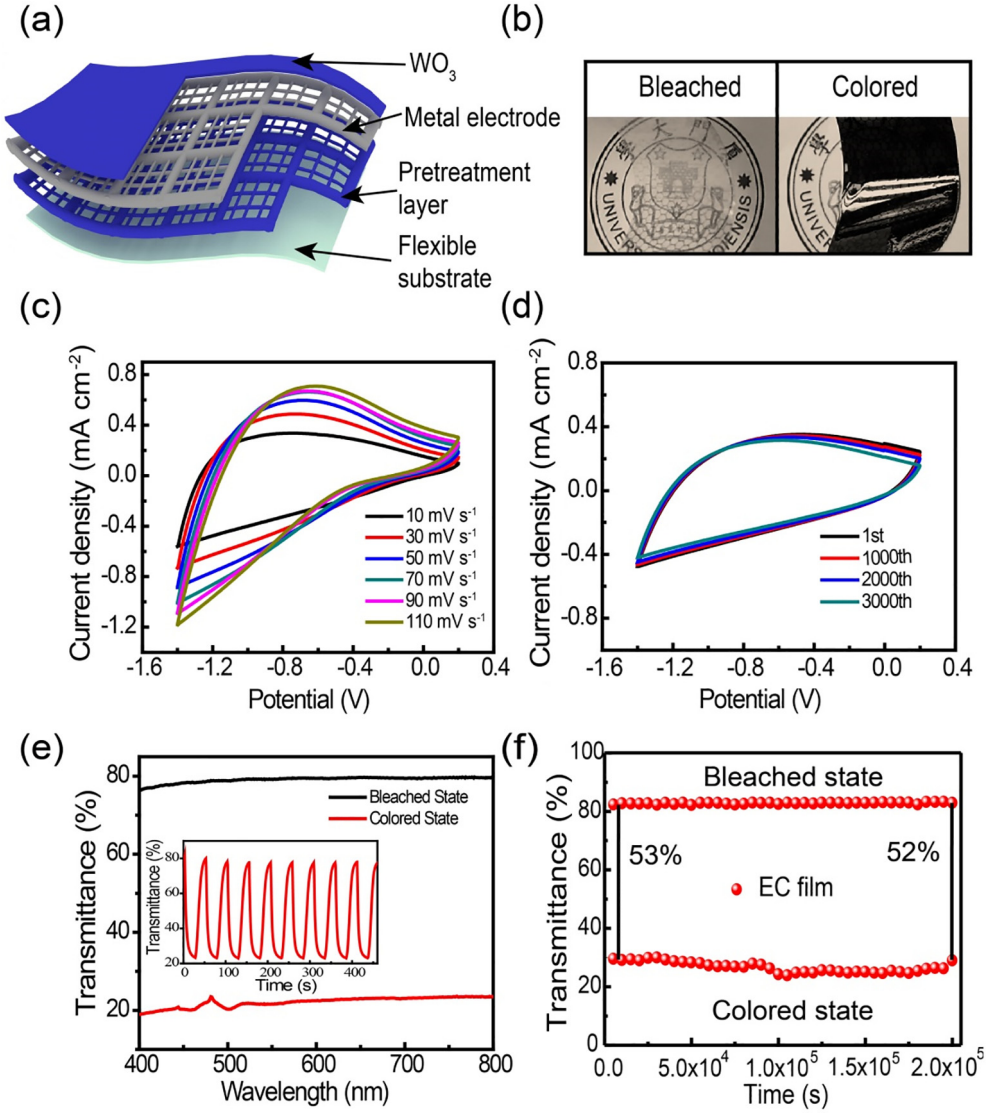

Fig. 6. (Color online) Fabrication and properties of the ECD. (a) Structural schematic diagram of the WO_3/Ag HMG conductive film. (b) Digital photographs of bleached and colored EC film. CV of the EC film was performed (c) at different potential scanning rates from 10 to 110 mV s^{-1} and (d) at a scanning rate of 10 mV s^{-1} over a potential range of –1.4 (colored) to 0.2 V (bleached). (e) The transmittance of the EC film between 400 and 800 nm in bleached and colored state, and the inset demonstrates the relationship between the working time and the transmittance of the EC film. (f) The optical contrast changes from initial to 2 × 10^5 s in bleached state and colored state with a potential change of 0.55 V.

According to the CV curves, the typical WO_3 redox peak and the position of the anodic and cathodes peaks were influenced by the charge which is stored at the surface of the electrodes in the processes of electrochemistry. The insertion (extraction) of Li^+ into (out of) the WO_3 leads to the change between colored and bleached state reversibly. The cycling performance as shown in Fig. 6d indicates the insertion and extraction of Li^+ have good reversibility, stability and durability. Fig. 6e shows the transmittance spectra of the EC film in the colored state and the bleached state, respectively, indicating the stable optical contrast through the spectra of the visible light in a range of 400–800 nm. The inset in Fig. 6e shows the relationship between the voltage sweep time and the transmittance of the EC film, the switching time for coloring and bleaching are 6.8 and 14.7 s respectively, with the voltages of –1.4 (coloration) and 0.2 V (bleaching). Apart from switching times, the cycling life is also important for the application of ECDs in smart window. As evident from Fig. 6f, after 2×10^5 s test in the aforementioned three-electrode system, almost no change was observed at optical contrast (from 53% to 52%), indicating high cycling stability of the ECD at the bleached and colored state, which is comparable to the previous reported works as shown in Table S1 (online) [37–39].

4. Conclusions

In this study, leaf vein-like hierarchical Ag grids FTCEs were successfully fabricated by simply lase-etching the self-cracked TiO_2 colloid patterns. The optoelectronic performance of the HMG film could be simply enhanced through adjusting the widths, shapes, spaces, and the sizes of the TiO_2 colloidal crackle patterns. The WO_3-Ag HMG electrodes produced in this way exhibited low sheet resistance (1.36 Ω sq^{-1}) at high optical transmittance (~81%), and a remarkable mechanical flexibility. In addition, the as-prepared flexible HMG electrodes were successfully utilized as TCEs in flexible ECDs, demonstrating superior cyclic performance.

Conflict of interest

The authors declare that they have no conflict of interest.

Acknowledgments

This work was supported by the Shenzhen Basic Research Program (JCYJ20180306173007696), the Natural Science Foundation of Fujian Province (2017J01104), the Fundamental Research Funds for the Central Universities of China (20720160127, 20720180013), Doctoral Fund of the Ministry of Education (20130121110018), NUS AcRF Tier 1 (R-144-000-367-112), the "111" Project (B16029) and the 1000 Talents Program Funding from the Xiamen University. The authors also thank the technical supports from Shengshi Guo, Rui Yu, Hao Wang and Likun Yang.

Author contributions

Shengyou Li and Teng Li designed and carried out the experiments. Shengyou Li, Xuyi Li and Zijie Xu conducted the materials characterization. Shengyou Li, Jizhong Zhao and Yating Shi performed the electrochemical test and analyses. Yanan Wang and Rui Yu finished XRD and XPS characterization. Xiangyang Liu, Qingchi Xu and Wenxi Guo provided the guidance for the whole research process and revised the paper. All authors discussed the results and commented on the manuscript.

Appendix A. Supplementary materials

Supplementary materials to this article can be found online at https://doi.org/10.1016/j.scib.2019.11.028.

References

[1] Hecht DS, Liangbing H, Glen I. Emerging transparent electrodes based on thin films of carbon nanotubes, graphene, and metallic nanostructures. Adv Mater 2011;23:1482–513.
[2] Blake P, Brimicombe PD, Nair RR, et al. Graphene-based liquid crystal device. Nano Lett 2008;8:1704–8.
[3] Junbo W, Mukul A, Becerril HA, et al. Organic light-emitting diodes on solution-processed graphene transparent electrodes. ACS Nano 2010;4:43–8.
[4] Wang J, Liang M, Fang Y, et al. Rod-coating: towards large-area fabrication of uniform reduced graphene oxide films for flexible touch screens. Adv Mater 2012;24:2874–8.
[5] Yang L, Zhang T, Zhou H, et al. Solution-processed flexible polymer solar cells with silver nanowire electrodes. ACS Appl Mater Interfaces 2011;3:4075–84.
[6] Guo W, Xu Z, Zhang F, et al. Recent development of transparent conducting oxide-free flexible thin-film solar cells. Adv Funct Mater 2016;26:8854.
[7] Gordon R. Criteria for choosing transparent conductors. MRS Bull 2000;25:52–7.
[8] Akshay K, Chongwu Z. The race to replace tin-doped indium oxide: which material will win?. ACS Nano 2010;4:11–4.
[9] Cairns DR, Witte RP, Sparacin DK, et al. Strain-dependent electrical resistance of tin-doped indium oxide on polymer substrates. Appl Phys Lett 2000;76:1425–7.
[10] Tahar RBH, Ban T, Ohya Y, et al. Tin doped indium oxide thin films: electrical properties. J Appl Phys 1998;83:2631–45.
[11] Xia Y, Sun K, Ouyang J. Solution-processed metallic conducting polymer films as transparent electrode of optoelectronic devices. Adv Mater 2012;24:2436–40.
[12] Luo B, Liu SM, Zhi LJ. Chemical approaches toward graphene-based nanomaterials and their applications in energy-related areas. Small 2012;8:630–46.
[13] Garrett M, Ivanov IN, Geohegan D, et al. Effect of purity on the electro-optical properties of single wall nanotube-based transparent conductive electrodes. Carbon 2013;64:1–5.
[14] Chen L, Hernandez Y, Feng X, et al. From nanographene and graphene nanoribbons to graphene sheets: chemical synthesis. Angew Chem Int Ed 2012;51:7640–54.
[15] Ko H, Mcnamee CE, Masaki N. Formation of large-scale flexible transparent conductive films using evaporative migration characteristics of Au nanoparticles. Langmuir 2011;27:2080–3.
[16] Han B, Pei K, Huang Y, et al. Uniform self-forming metallic network as a high-performance transparent conductive electrode. Adv Mater 2014;26:873–7.
[17] Ye S, Rathmell AR, Stewart IE, et al. A rapid synthesis of high aspect ratio copper nanowires for high-performance transparent conducting films. Chem Commun 2014;50:2562–4.
[18] Kang MG, Kim MS, Kim J, et al. Organic solar cells using nanoimprinted transparent metal electrode. Adv Mater 2010;20:4408–13.
[19] Park JH, Lee DY, Kim YH, et al. Flexible and transparent metallic grid electrodes prepared by evaporative assembly. ACS Appl Mater Interfaces 2014;6:12380–7.
[20] Song M, Kim HJ, Chang SK, et al. ITO-free highly bendable and efficient organic solar cells with Ag nanomesh/ZnO hybrid electrodes. J Mater Chem A 2014;3:65–70.
[21] Jin Y, Cheng Y, Deng D, et al. Site-selective growth of patterned silver grid networks as flexible transparent conductive film by using poly(dopamine) at room temperature. ACS Appl Mater Interfaces 2014;6:1447–53.
[22] Lee Y, Jin W, Cho KY, et al. Thermal pressing of a metal-grid transparent electrode into a plastic substrate for flexible electronic devices. J Mater Chem C 2016;4:7577–83.
[23] Gao JW, Kempa K, Giersig M, et al. Physics of transparent conductors. Adv Phys 2016;65:553–617.
[24] Cai G, Darmawan P, Cui M, et al. Highly stable transparent conductive silver grid/PEDOT:PSS electrodes for integrated bifunctional flexible electrochromic supercapacitors. Adv Energy Mater, 6: 1501882
[25] Qiu T, Luo B, Liang M, et al. Hydrogen reduced graphene oxide/metal grid hybrid film: towards high performance transparent conductive electrode for flexible electrochromic devices. Carbon 2015;81:232–8.
[26] Yan G, Le Y, Wang CA, et al. Hierarchical tubular structures composed of mn-based mixed metal oxide nanoflakes with enhanced electrochemical properties. Adv Funct Mater 2015;25:5184–9.
[27] Wu H, Kong D, Ruan Z, et al. A transparent electrode based on a metal nanotrough network. Nat Nanotechnol 2013;8:421–5.
[28] Lee MS, Lee K, Kim SY, et al. High-performance, transparent, and stretchable electrodes using graphene-metal nanowire hybrid structures. Nano Lett 2013;13:2814–21.
[29] Li L, Zhang B, Zou B, et al. Fabrication of flexible transparent electrode with enhanced conductivity from hierarchical metal grids. ACS Appl Mater Interfaces 2017;9:39110–5.

[30] Hsu PC, Wang S, Wu H, et al. Performance enhancement of metal nanowire transparent conducting electrodes by mesoscale metal wires. Nat Commun 2013;4:2522.
[31] Han B, Huang Y, Li R, et al. Bio-inspired networks for optoelectronic applications. Nat Commun 2014;5:5674.
[32] Gao JW, Xian ZK, Zhou GF, et al. Nature-inspired metallic networks for transparent electrodes. Adv Funct Mater 2018;28:1705023.
[33] Rao KDM, Kulkarni GU. A highly crystalline single Au wire network as a high temperature transparent heater. Nanoscale 2014;6:5645–51.
[34] Liu Q, Xu Z, Qiu W, et al. Ultraflexible, stretchable and fast-switching electrochromic devices with enhanced cycling stability. RSC Adv 2018;8:18690–7.
[35] Liu W, Fang Y, Li X, et al. Effect of grid shape on properties of metal grid transparent conductive film. China Print Packag Study 2014;6:112–7.
[36] Khan A, Lee S, Jang T, et al. High-performance flexible transparent electrode with an embedded metal mesh fabricated by cost-effective solution process. Small 2016;12:3021–30.
[37] Zhong Y, Chai Z, Liang Z, et al. Electrochromic asymmetric supercapacitor windows enable direct determination of energy status by the naked eye. ACS Appl Mater Interfaces 2017;9:34085–92.
[38] Cai G, Cheng X, Layani M, et al. Direct inkjet-patterning of energy efficient flexible electrochromics. Nano Energy 2018;49:147–54.
[39] Yun TG, Park M, Kim D, et al. All-transparent stretchable electrochromic supercapacitor wearable patch device. ACS Nano 2019;13:3141–50.

Shengyou Li is a master student in the Research Institute for Soft Matter and Biomimetics, College of Physical Science and Technology at Xiamen University. He received his Bachelor degree in College of Materials Science and Engineering from University of Jinan in 2018. His research interests include flexible ITO-free conductive films and silk-based flexible electronic devices.

Qingchi Xu obtained his Bachelor degree (2003) and Ph. D. degree (2008) at Xiamen University. He was a post-doctoral fellow at Nanyang Technological University in Singapore (2008–2011, 2014). Currently, he is an Associate Professor at Research Institute for Soft Matter and Biomimetics and Department of Physics at Xiamen University. His research interests focus on multifunctional nanomaterial-based synthesis for energy and environment applications, such as photocatalysis, flexible electronics, lithium ion battery and heterogeneous catalysis.

Wenxi Guo received his B.S. and Ph.D. degrees in College of Chemistry and Chemical Engineering at Xiamen University in 2008 and 2014, respectively. Then, he had been an assistant research fellow in the group of Prof. Caofeng Pan at Beijing Institute of Nanoenergy and Nanosystems, Chinese Academy of Sciences. He then joined School of Physics and Technology, Xiamen University and became an Associate Professor in 2015. His research focuses on the fields of flexible thin film solar cells, flexible electronic devices, and piezotronic/piezophototronic effects of nanodevices.